

Relativistic VQE calculations of molecular electric dipole moments on trapped ion quantum hardware

Palak Chawla,^{1,*} Shweta,^{2,*} K. R. Swain,^{1,†} Tushti Patel,¹ Renu Bala,^{1,‡} Disha Shetty,¹ Kenji Sugisaki,^{1,3,4,5} Sudhindu Bikash Mandal,¹ Jordi Riu,^{6,7} Jan Nogué,⁶ V. S. Prasanna,^{1,8,§} and B. P. Das^{1,8,9}

¹Centre for Quantum Engineering, Research and Education, TCG Crest, Kolkata 700091, India

²Department of Physics, Indian Institute of Technology Delhi, New Delhi 110016, India

³Graduate School of Science and Technology, Keio University,

7-1 Shinkawasaki, Saiwai-ku, Kawasaki, Kanagawa 212-0032, Japan

⁴Quantum Computing Center, Keio University, 3-14-1 Hiyoshi,
Kohoku-ku, Yokohama, Kanagawa 223-8522, Japan

⁵Keio University Sustainable Quantum Artificial Intelligence Center (KSQAIC),
Keio University, 2-15-45 Mita, Minato-ku, Tokyo, Japan

⁶Qilimanjaro Quantum Tech, Carrer dels Comtes de Bell-Lloc, 161, 08014 Barcelona, Spain

⁷Universitat Politècnica de Catalunya, Carrer de Jordi Girona, 3, 08034 Barcelona, Spain

⁸Academy of Scientific and Innovative Research (AcSIR), Ghaziabad- 201002, India

⁹Department of Physics, Tokyo Institute of Technology,
2-12-1 Ookayama, Meguro-ku, Tokyo 152-8550, Japan

(Dated: September 17, 2024)

The quantum-classical hybrid variational quantum eigensolver (VQE) algorithm is among the most actively studied topics in atomic and molecular calculations on quantum computers, yet few studies address properties other than energies or account for relativistic effects. This work presents high-precision 18-qubit relativistic VQE simulations for calculating the permanent electric dipole moments (PDMs) of BeH to RaH molecules on traditional computers, and 6- and 12-qubit PDM computations for SrH on IonQ quantum devices. To achieve high precision on current noisy intermediate scale era quantum hardware, we apply various resource reduction methods, including Reinforcement Learning and causal flow preserving ZX-Calculus routines, along with error mitigation and post-selection techniques. Our approach reduces the two-qubit gate count in our 12-qubit circuit by 99.71%, with only a 2.35% trade-off in precision for PDM when evaluated classically within a suitably chosen active space. On the current generation IonQ Forte-I hardware, the error in PDM is -1.17% relative to classical calculations and only 1.21% compared to the unoptimized circuit.

I. INTRODUCTION

The quantum-classical hybrid Variational Quantum Eigensolver (VQE) algorithm, which is built on the Rayleigh-Ritz variational principle, is the leading approach to calculating energies in the Noisy Intermediate Scale Quantum (NISQ) era [1–17]. VQE is an iterative procedure, which involves minimizing an energy functional through energy evaluations on a quantum device and parameter updates on a traditional computer, that yields an upper bound to the true ground

state energy [18]. In particular, given a Hamiltonian, \hat{H} , and a suitably parametrized state, $|\Psi(\theta)\rangle$, where $\{\theta\} \in \{\theta_1, \theta_2, \dots\}$, minimizing an energy functional $E(\theta) = \frac{\langle \Psi(\theta) | \hat{H} | \Psi(\theta) \rangle}{\langle \Psi(\theta) | \Psi(\theta) \rangle} = \langle \Phi | U^\dagger(\theta) \hat{H} U(\theta) | \Phi \rangle$ with respect to $\{\theta\}$ yields an optimized state, $|\Psi(\theta^*)\rangle$, such that $\langle \Phi | U^\dagger(\theta) \hat{H} U(\theta) | \Phi \rangle \geq E_0$. Here, the state $|\Psi(\theta)\rangle$ is expressed as a unitary, $U(\theta)$ acting on a reference state (which for our purposes is the Hartree-Fock/Dirac-Fock (DF) state), $|\Phi\rangle$. The VQE approach, by construction, leads to relatively low-depth quantum circuits [1], thus making it the workhorse for atomic and molecular calculations in the NISQ era.

Despite its successes, the algorithm remains limited in its applications: it is mainly employed to calculate ground state energies, ionization energies, and excitation energies [19–25], whereas VQE’s application to other properties, like the molecular permanent electric dipole moments (PDMs), is limited [21, 26, 27]. There is also little in VQE literature on extending it to the relativistic

* Contributed equally to the work

† Current address: Department of Physics and Materials Science, University of Luxembourg, L-1511 Luxembourg, Luxembourg

‡ Current address: Institute of Physics, Faculty of Physics, Astronomy and Informatics, Nicolaus Copernicus University, Grudziadzka 5, 87-100 Toruń, Poland

§ srinivasaprasanna@gmail.com

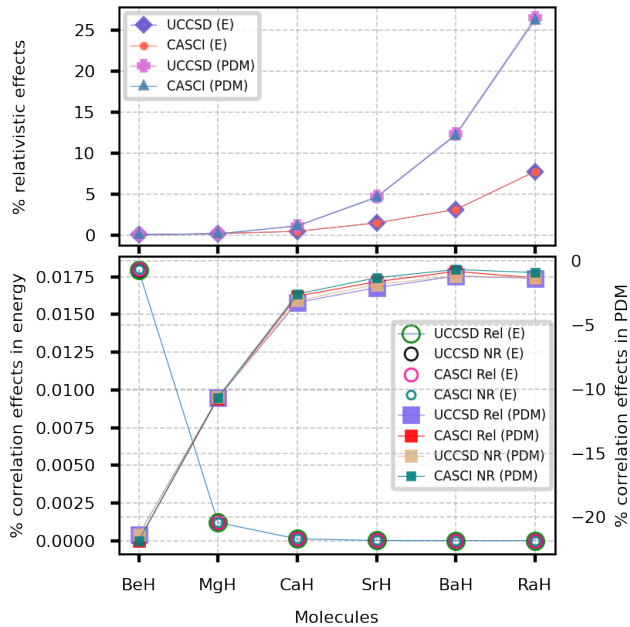


Figure 1. The top panel shows the percentage relativistic effects $= \frac{A_{Rel} - A_{NR}}{A_{Rel}} \times 100$ for ground state energy (E) and PDM from our 18-qubit VQE simulations. Our results are benchmarked against CASCI calculations. The bottom panel shows the percentage correlation effects $= \frac{A_X - A_{ME}}{A_X} \times 100$, where X can be correlation energy (circular markers) or the PDM (square markers) relative to respective quantity at VQE and CASCI levels.

regime [28]. In fact, there are only a handful of studies that incorporate relativistic effects in the context of even other quantum algorithms [29–32]. The inclusion of relativity in atomic and molecular physics calculations has led to several notable predictions, including explaining the colour of gold [33], relativistic contraction of bond lengths [33], and the rationale behind starting of cars with lead-acid batteries [34]. A vast landscape of atomic and molecular properties where relativity is important, ranging from practically useful atomic clocks to probing particle physics [35–46], remains to be explored. Therefore, given the gap in the otherwise extensive VQE literature in (a) calculating atomic and molecular properties other than energy, and (b) the potential opened by including relativistic effects, a study of molecular properties using relativistic VQE is timely.

We focus on the molecular electric dipole moment (PDM), which is particularly useful in several applications, including the search for novel quantum phases like the supersolid phase [47], study of dipole–dipole molecular interactions with implications in quantum computing

[48], and fundamental physics searches [49]. In particular, the PDMs of the alkaline earth metal monohydrides are of significant interest due to their potential for laser cooling [50, 51]. Notably, CaH and BaH have already been laser-cooled [52, 53].

Despite the limitations of quantum hardware in the NISQ era, it is crucial to push the boundaries of the current best available technology. This effort would not only showcase the progress made but also would provide insights into advancements and directions for exploring quantum algorithms and hardware in the near-term. To that end, we compute the PDM of the moderately heavy SrH molecule in a 12-qubit relativistic VQE calculation on among the best available commercial quantum computers, the current generation IonQ Forte-I device. Typical VQE calculations on quantum hardware using the physics/chemistry-inspired unitary coupled cluster (UCC) ansatz employ resource reduction strategies to minimize qubits, gates, and VQE iterations, along with error mitigation techniques, to predict energies [2, 54–60]. The largest such computation carried out to date involved 12-qubits [2], but the framework was non-relativistic and the property of interest was the ground state energy. In this work, we conduct 12-qubit relativistic VQE computations of the PDM, but due to the deep circuits incurred for such tasks, a significant part of our effort focuses on resource reduction. This allows us to achieve sufficiently shallow circuit depths for reasonable precision, while carefully preserving the underlying physics to the best capabilities of NISQ computers.

II. THEORY AND METHODOLOGY

We now discuss some details of the VQE algorithm to calculate the PDM. The quality of a VQE calculation is predominantly determined by choice of $U(\theta)$. We choose the UCC ansatz for $U(\theta)$, which being both variational and unitary, is well-suited for quantum computers while retaining the predictive accuracy of traditional CC methods, which are deemed to be the gold standard of electronic structure calculations [61]. The UCC ansatz is given by $|\Psi(\theta)\rangle = e^{\hat{T} - \hat{T}^\dagger} |\Phi\rangle = e^{\hat{T}} |\Phi\rangle$. The ansatz includes single (\hat{T}_1) and double (\hat{T}_2) excitations (UCCSD approximation): $\hat{T}_1 = \sum_{ia} \theta_i^a \hat{a}_i^\dagger \hat{a}_i$, $\hat{T}_2 = \sum_{ijab} \theta_{ij}^{ab} \hat{a}_i^\dagger \hat{a}_j^\dagger \hat{a}_b \hat{a}_i$. i, j, \dots indicate indices of occupied spinorbitals, while a, b, \dots are those of unoccupied/virtual ones. We note that the Hamiltonian is given by $\hat{H} = \sum_{pq} h_{pq} \hat{a}_p^\dagger \hat{a}_q + \frac{1}{2} \sum_{pqrs} h_{pqrs} \hat{a}_p^\dagger \hat{a}_q^\dagger \hat{a}_s \hat{a}_r$ in the second quantized notation, where h_{pq} and h_{pqrs} are the one- and two-electron integrals, and p, q, \dots can denote indices

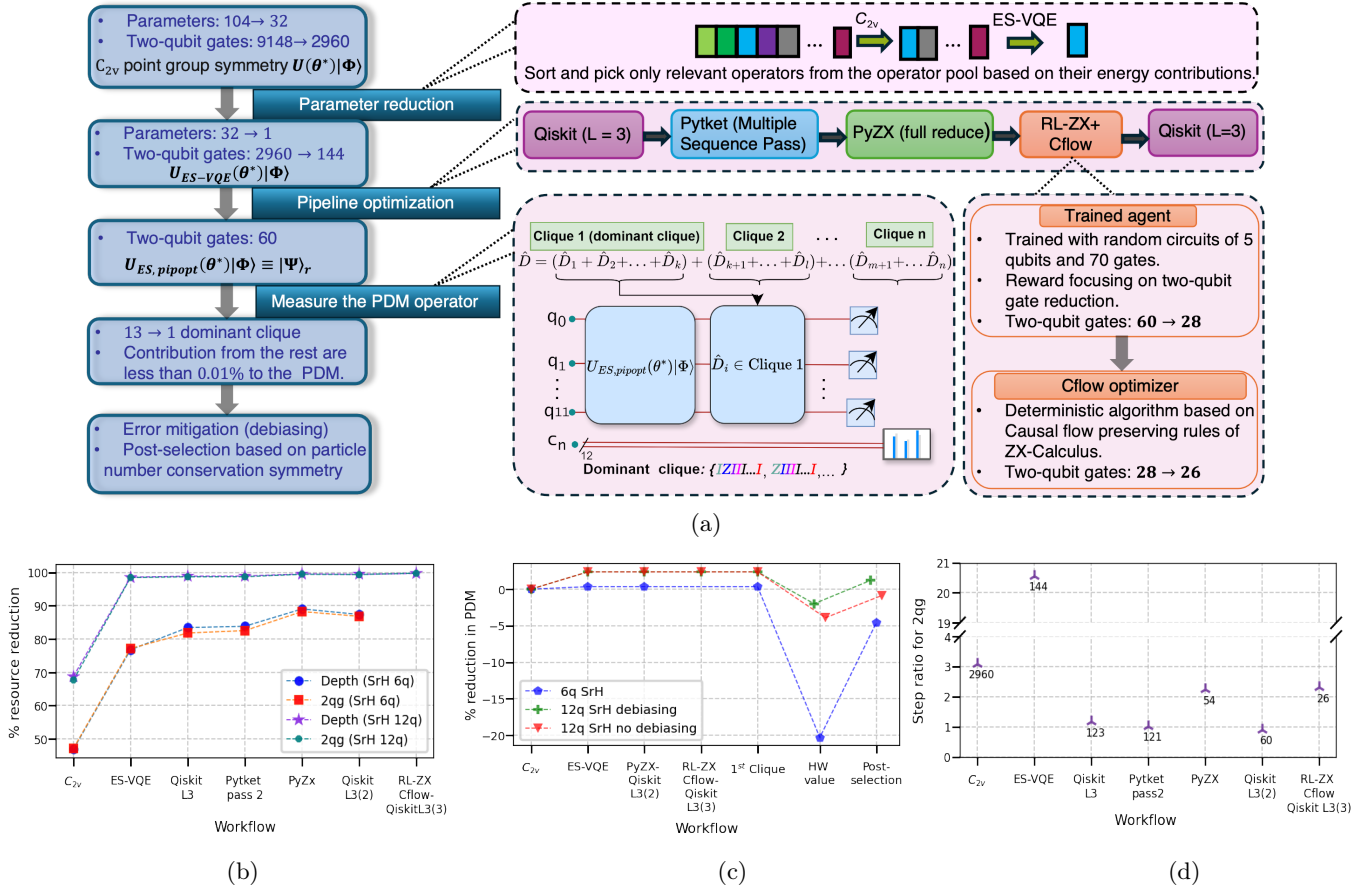


Figure 2. (a) Our workflow for quantum hardware execution of SrH 12-qubit PDM calculation on the IonQ Forte device, which leads to reducing quantum resources while retaining precision. (b) Percentage reduction in resources (two-qubit gates, denoted as 2qg in the sub-figure, and circuit depth) with each step of our workflow: U_{ES-VQE} is the UCCSD circuit post-ES-VQE and $U_{ES, Pipopt}$ is the state after pipeline-based optimization (denoted as pipopt). (c) The loss of precision in predicting PDM after each step in our workflow, with ‘1st Clique’ indicating the selection of the dominant clique for the PDM operator (See Table S3 of the Supplemental Material). Sub-figure (d) illustrates the step ratio, which is the ratio of the number of 2qg before and after the current step in our workflow. It is important to stress that the compound strategy of our RL-ZX based agent followed by the causal flow deterministic algorithm (both based on ZX-Calculus, denoted as RL-ZX + Cflow) reduces the already small gate count by one half.

of occupied or unoccupied spinorbitals. Upon using the Jordan–Wigner transformation [62] for both the state and the Hamiltonian, the energy functional can be expressed as $E(\theta) = \sum_m^M \alpha_m \langle \Phi' | U'^{\dagger}(\theta) \hat{P}_m U'(\theta) | \Phi' \rangle$. $U'(\theta)$ and $|\Phi'\rangle$ refer to the Jordan–Wigner-transformed $U(\theta)$ and $|\Phi\rangle$, respectively. α_m are the coefficients depending on h_{pq} and h_{pqrs} and P_m are Pauli strings represented by tensor products of Pauli operators $\{I, X, Y, Z\}$. Each term in the equation corresponds to the expectation value of a Pauli string \hat{P}_m , which is evaluated through statistical sampling on a quantum computer, while the summation and energy minimization is done on a traditional com-

puter. Once the optimized parameters are determined, we evaluate $\sum_n^N d_n \langle \Phi' | U'^{\dagger}(\theta^*) \hat{P}_n U'(\theta^*) | \Phi' \rangle$, where d_n are coefficients that depend on the PDM integrals and \hat{P}_n here are Pauli strings that arise from the transformation of the PDM operator from the second quantized to its qubit operator form. Since we carry out our calculations in an active space, we add to this quantity the frozen core PDM contribution along with the usual nuclear contribution, to obtain the total PDM. For the relativistic calculations, we employ the Dirac–Coulomb Hamiltonian in the Born–Oppenheimer approximation, given by

$\hat{H}_{DC} = \sum_k (c\vec{\alpha} \cdot \vec{p}_k + \beta c^2) + \sum_k V_{nuc}(r_k) + \frac{1}{2} \sum_{k \neq l} \frac{1}{r_{kl}}$, where $\vec{\alpha} = \begin{pmatrix} 0 & \vec{\sigma} \\ \vec{\sigma} & 0 \end{pmatrix}$, $\beta = \begin{pmatrix} \mathbb{I} & 0 \\ 0 & -\mathbb{I} \end{pmatrix}$, $\vec{\sigma}$ are the Pauli matrices and \mathbb{I} is the (2×2) identity matrix. The summations are over the number of electrons. $V_{nuc}(r_k)$ refers to the electron–nucleus potential. We use finite-sized nuclei (Gaussian) for our relativistic calculations. We report all our results in atomic units (au), unless specified otherwise.

We use the following equilibrium bond lengths (in Å): BeH: 1.342 [63], MgH: 1.7297 [63], CaH: 2.0025 [63], SrH: 2.1461 [63], BaH: 2.2319 [63], and RaH: 2.43 [64]. The one- and two-electron integrals, as well as property integrals, are generated by the DIRAC22 program [65]. The VQE-UCCSD statevector computations are performed using Qiskit [66], interfaced via modified OpenFermion–Dirac libraries [65]. We use uncontracted dyall.v4z basis sets for our simulations [67]. First the parameters for VQE computations are initialized with zero initial guesses and parameters in each iteration are updated using the SLSQP (Sequential Least Squares Programming) optimizer [68]. We adopt the Jordan–Wigner mapping scheme throughout and benchmark our VQE-UCCSD PDM values against complete active space configuration interaction (CASCI) calculations, where the Jordan–Wigner-transformed qubit Hamiltonian is diagonalized with the correct particle number using the OpenFermion package [69].

Relativistic VQE calculations require more quantum resources than their non-relativistic counterparts. The number of circuit evaluations in VQE scales as the product of Hamiltonian terms and iterations (we ignore the number of shots and number of repetitions of an experiment). Relativistic calculations have more non-zero Hamiltonian integrals, resulting in more circuits to evaluate. In the 18-qubit RaH calculation, relativistic VQE requires 12556 Pauli strings (47099 integrals) for the Hamiltonian and 107 (162 integrals) for the PDM operator, compared to 2740 (4249 integrals) and 67 (66 integrals) for the non-relativistic cases, indicating that relativistic VQE is more resource-intensive.

III. RESULTS AND DISCUSSIONS

We now discuss our findings from our 18-qubit VQE simulations (3 occupied and 15 unoccupied spinorbitals). The top panel of Figure 1 illustrates the size of relativistic effects, quantified as % relativistic effects = $\frac{A_{Rel} - A_{NR}}{A_{Rel}} \times 100$, where A represents either the ground state energy or the PDM (see Table S1 of the Appendix

for data). It shows that relativistic effects increase significantly from BeH to RaH, with relativity accounting for 7.73% of the ground state energy and 26.47% of the PDM in RaH. Further, VQE-UCCSD and the reference CASCI results disagree by at most 0.47% (for CaH). We note that for BaH (non-relativistic case), the HF calculation initially converged to a metastable spin-doublet state. We obtained the lowest spin-doublet HF state by replacing the initial guess orbitals with HF canonical orbitals from a neighboring geometry. We also note that our PDM results for BeH and MgH are in reasonably good agreement with high-accuracy calculations, with percentage differences of 2.05% and 3.79% respectively, which may be attributed to our active space sizes and basis set quality. We now examine the role of correlation effects. The bottom panel of Figure 1 shows the % correlation effects, defined as $\frac{A_X - A_{MF}}{A_X} \times 100$, for both properties. Here, A can be either the ground state energy or the PDM, and X can be VQE-UCCSD or CASCI. MF is HF for non-relativistic cases and DF for relativistic calculations. The figure shows that the VQE-UCCSD and CASCI results agree remarkably well in predicting correlation energy, within 0.0175%. It also shows that VQE-UCCSD and CASCI values are consistent in their prediction of the correlation contribution to the PDM. To understand the interplay between relativistic and correlation effects, we focus on the heaviest RaH molecule. Relativistic effects significantly impact RaH’s PDM. Correlation effects decrease its PDM by 1.32% and 1.36% for non-relativistic and relativistic cases, respectively. Conversely, relativity increases the PDM by 26.50% at the mean field level and 26.47% at the correlated level. The combined effect changes the PDM from 1.1306 to 1.5177 atomic units, a total change of 25.51%.

Quantum hardware computations: We compute the active space PDM, henceforth abbreviated as PDM_{as} (the value of the quantity before we manually add the frozen core contributions and nuclear contribution to obtain the total PDM), of SrH in the STO-6G basis in a 12-qubit active space on the IonQ Forte-I device (average 2-qubit gate fidelity: 98.99%), and also perform 6-qubit active space PDM calculations for SrH and SrF on the IonQ Aria-I device (average 2-qubit gate fidelity: 98.43%). Since PDM_{as} is what we measure in hardware and thus the errors incurred in hardware reflect changes to this quantity, we only report it in our figures (see Table S2 of the Appendix for the total PDM values). Despite Forte-I being among the best available commercial quantum computers, achieving high precision on current noisy hardware requires a workflow with several resource reduction techniques, as illustrated in Figure 2. In particular, sub-

figures (b) through (d) present data on the quantum resource reduction, the trade-off in the active space PDM, and the ratio of the number of 2-qubit gates ($2qg$) in the previous step to current step. We outline our workflow below:

- 1. Point group symmetry:** Leveraging the C_{2v} point group symmetry [70] reduces the number of coupled cluster amplitudes, and hence the number of VQE parameters, from 8 to 3 and $2qg$ from 280 to 148 for the 6-qubit case. On the other hand, in the 12-qubit circuit, the number of parameters reduce from 104 to 32 and $2qg$ reduces from 9148 to 2960.
- 2. Energy Sort VQE (ES-VQE):** The ES-VQE approach [71] involves carrying out one-parameter VQEs and sorting in descending order the resulting energies, and then carrying out VQE calculations with progressively increasing number of parameters chosen according to the sort. For our purposes, given current-day quantum hardware limitations but also keeping in mind our need to achieve high precision, we pick the parameter with dominant energy contribution for both the 6- and 12- qubit cases (double excitation from (1,3) orbital to (2,5) orbital and from (1,7) to (5,11) orbital for the 6- and 12-qubit examples respectively). We note that we chose 3 and 5 occupied spinorbitals for the 6- and 12-qubit computations respectively. This process reduces $2qg$ further to 64, with only a 0.33% loss in PDM for SrH, for the 6-qubit computations. For the 12-qubit case, $2qg$ goes from 2960 to 144, while retaining precision in the PDM_{as} to within 97.65%.
- 3. Pipeline-based optimization:** A sequence of optimization routines (Qiskit L3 [66], Pytket [72], PyZX [73]) further decreases $2qg$ in the 6- and 12-qubit circuits to 37 and 60 respectively. We incur no loss in the PDMs during this step.
- 4. Reinforcement learning (RL) aided and causal flow preserving ZX-Calculus based approaches:** As a final optimization, we followed the approach described in Ref. [74], where an agent is trained using RL and Graph Neural Networks to apply ZX-Calculus-based graph-theoretic rules for circuit optimization. In this work, we trained our agent with random 5- qubit circuits with 70 $2qg$, but with similar gate probabilities as the 12-qubit target circuit. Moreover we defined the reward to focus on $2qg$ reduction. For the 12q case, the agent managed to reduce the $2qg$ from 60 to 28. As a post-processing step, we added the deterministic algorithm from Ref. [75] based on causal flow preserving

rules of ZX-Calculus, which in turn reduces the previous $2qg$ by 2. We incur no loss in PDM after this step.

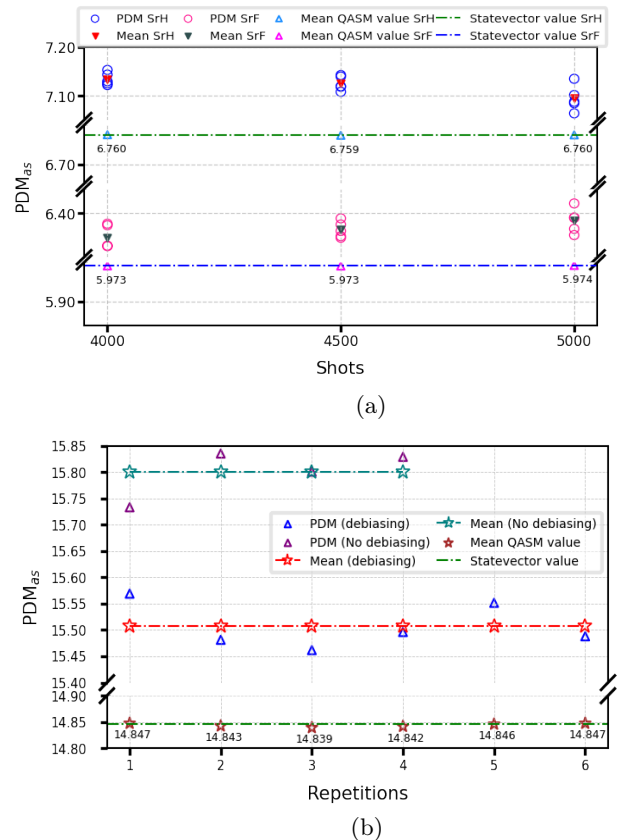


Figure 3. Active space PDM (PDM_{as}) results (in atomic units) for (a) SrH and SrF molecules in a 6-qubit active space with varying shot numbers, averaged over five repeats (each repeat is denoted by a circle, and the average value by a solid variant of ‘ ∇ ’), obtained on the 25-qubit IonQ Aria-I hardware after error mitigation and post-selection. The data points denoted with a star symbol give the mean values obtained using the QASM backend on a traditional computer, while the dashed-dotted lines are the statevector results. We note that the main results reported in text take data from the 5000 shots calculation. Sub-figure (b) presents our 12-qubit results on the IonQ Forte-I device for PDM_{as} of SrH across repetitions with and without error mitigation.

- 5. Qubit-wise commuting Pauli groups:** The 6- and 12- qubit PDM computations each involve computing expectation values of 19 and 53 terms respectively, and hence evaluating as many circuits. By partitioning the qubit operator for the PDM into qubit-wise commuting cliques followed by selecting and measuring only the

dominant clique (and hence evaluating only one circuit for 6-qubit case and one for the 12-qubit counterpart) for quantum hardware computation, we find that we achieve substantial reduction in the resources with no loss in PDM.

6. Error mitigation and post-selection: We use the debiasing error mitigation method [76], followed by post-selecting the particle number conserving bit strings to obtain the PDM_{as} [77, 78].

6- qubit calculation on PDM on IonQ Aria-I: We discuss results from our quantum hardware computations on the Aria-I device for SrH and SrF molecules. Figure 3(a) show the values of PDM_{as} , with error-mitigated and post-selected results averaged over 5 repetitions for both the molecules, across different numbers of shots. Considering the computations with 5000 shots as our main result, we see that the percentage fraction difference with respect to statevector results is about 4.94% for SrH and 6.90% for SrF. The 2-qubit gate fidelity was around 98.43%.

12- qubit calculation on PDM on IonQ Forte-I: Figure 3(b) presents our results for the PDM_{as} of the SrH molecule across different repetitions, with and without error mitigation (debiasing). We find that the mitigated value of the average PDM_{as} that we obtain across 6 repeats is to within 98.81% of the mean QASM value. The figure also indicates that mitigation improves the result by 2.11% relative to the mean QASM value.

IV. CONCLUSION

In conclusion, considering the existing gap in the VQE literature concerning the inclusion of relativistic effects and the calculation of properties beyond energies, we implement a relativistic VQE algorithm for calculating molecular permanent electric dipole moments of polar diatomic molecules from BeH to RaH. Benchmarking our 18-qubit VQE simulation results against the complete active space configuration interaction method provides valuable insights into the roles as well as the interplay between correlation and relativistic effects. We achieve a precision of at least 99.72% in capturing relativistic effects for the RaH molecule with respect to the CASCI value.

Furthermore, we perform high precision quantum hardware computations of the molecular electric dipole moments of the moderately heavy SrH (6- and 12-qubit calculations) and SrF (6-qubit calculation) systems. We employ strategies including point group symmetry, energy sort VQE, pipeline based circuit optimization, reinforcement learning- based ZX-Calculus, and causal flow preserving ZX-Calculus for the 12-qubit computation to compress the circuit by 99.71%. We also use debiasing for error mitigation followed by particle number conserving post-selection, to reach a precision of 95.06% and 93.10% (relative to the result obtained by executing the same circuit without noise on a classical device) for the 6-qubit computations on SrH and SrF respectively, and 98.82% for the 12-qubit SrH calculation. This work marks a significant advancement in high-precision relativistic VQE computations, and we expect future progress in quantum hardware to extend these methods to heavier molecular systems and new applications in probing fundamental physics.

ACKNOWLEDGMENTS

Calculations were performed on the Rudra cluster (SankhyaSutra Labs) and on the Airawat cluster, CDAC Pune. KS acknowledges support from Quantum Leap Flagship Program (Grant No. JPMXS0120319794) from the MEXT, Japan, Center of Innovations for Sustainable Quantum AI (JPMJPF2221) from JST, Japan, and Grants-in-Aid for Scientific Research C (21K03407) and for Transformative Research Area B (23H03819). BPD and VSP acknowledge support from MeitY-AWS Braket QCAL project (N-21/17/2020-NeGD, 2022-24). We would like to acknowledge Dr. V. P. Majety (IIT Tirupati) for useful discussions. Shweta acknowledges Dr. Bodhaditya Santra and members of CAQT lab (IIT Delhi) for their support during completion of this project. VSP acknowledges support from Mr. Nishanth Baskaran, Dr. Anjani Priya, Dr. Jean-Christophe and Dr. Daniela for support related to AWS Braket execution. PC acknowledges Mr. Peniel B. Tsemo for useful discussions.

[1] A. Peruzzo, J. McClean, P. Shadbolt, M.-H. Yung, X.-Q. Zhou, P. J. Love, A. Aspuru-Guzik, and J. L. O'Brien, Nature Communications **5**, 4213 (2014).
 [2] S. Guo, J. Sun, H. Qian, M. Gong, Y. Zhang, F. Chen,

Y. Ye, Y. Wu, S. Cao, K. Liu, *et al.*, Nature Physics **20**, 1240 (2024).
 [3] C. Ying, B. Cheng, Y. Zhao, H.-L. Huang, Y.-N. Zhang, M. Gong, Y. Wu, S. Wang, F. Liang, J. Lin, Y. Xu,

- H. Deng, H. Rong, C.-Z. Peng, M.-H. Yung, X. Zhu, and J.-W. Pan, *Physical Review Letters* **130**, 110601 (2023).
- [4] T. E. O'Brien, G. Anselmetti, F. Gkritis, V. Elfving, S. Polla, W. J. Huggins, O. Oumarou, K. Kechedzhi, D. Abanin, R. Acharya, *et al.*, *Nature Physics* **19**, 1787 (2023).
- [5] K. Yamamoto, D. Z. Manrique, I. T. Khan, H. Sawada, and D. M. Ramo, *Physical Review Research* **4**, 033110 (2022).
- [6] A. Eddins, M. Motta, T. P. Gujarati, S. Bravyi, A. Mezzacapo, C. Hadfield, and S. Sheldon, *PRX Quantum* **3**, 010309 (2022).
- [7] Q. Gao, G. O. Jones, M. Motta, M. Sugawara, H. C. Watanabe, T. Kobayashi, E. Watanabe, Y.-y. Ohnishi, H. Nakamura, and N. Yamamoto, *npj Computational Materials* **7**, 70 (2021).
- [8] Y. Kawashima, E. Lloyd, M. P. Coons, Y. Nam, S. Matsuura, A. J. Garza, S. Johri, L. Huntington, V. Senicourt, A. O. Maksymov, *et al.*, *Communications Physics* **4**, 245 (2021).
- [9] G. A. Quantum, Collaborators, F. Arute, K. Arya, R. Babbush, D. Bacon, J. C. Bardin, R. Barends, S. Boixo, M. Broughton, B. B. Buckley, *et al.*, *Science* **369**, 1084 (2020).
- [10] Y. Nam, J.-S. Chen, N. C. Pient, K. Wright, C. Delaney, D. Maslov, K. R. Brown, S. Allen, J. M. Amini, J. Apisdorf, *et al.*, *npj Quantum Information* **6**, 33 (2020).
- [11] A. Kandala, K. Temme, A. D. Córcoles, A. Mezzacapo, J. M. Chow, and J. M. Gambetta, *Nature* **567**, 491 (2019).
- [12] A. J. McCaskey, Z. P. Parks, J. Jakowski, S. V. Moore, T. D. Morris, T. S. Humble, and R. C. Pooser, *npj Quantum Information* **5**, 99 (2019).
- [13] C. Hempel, C. Maier, J. Romero, J. McClean, T. Monz, H. Shen, P. Jurcevic, B. P. Lanyon, P. Love, R. Babbush, *et al.*, *Physical Review X* **8**, 031022 (2018).
- [14] J. I. Colless, V. V. Ramasesh, D. Dahlen, M. S. Blok, M. E. Kimchi-Schwartz, J. R. McClean, J. Carter, W. A. de Jong, and I. Siddiqi, *Physical Review X* **8**, 011021 (2018).
- [15] A. Kandala, A. Mezzacapo, K. Temme, M. Takita, M. Brink, J. M. Chow, and J. M. Gambetta, *Nature* **549**, 242 (2017).
- [16] P. J. O'Malley, R. Babbush, I. D. Kivlichan, J. Romero, J. R. McClean, R. Barends, J. Kelly, P. Roushan, A. Tranter, N. Ding, *et al.*, *Physical Review X* **6**, 031007 (2016).
- [17] J. Tilly *et al.*, *Physics Reports* **986**, 1 (2022).
- [18] S. H. Gould, *Variational Methods for Eigenvalue Problems* (University of Toronto Press, 1966).
- [19] M. Ostaszewski, E. Grant, and M. Benedetti, *Quantum* **5**, 391 (2021).
- [20] H. L. Tang, V. Shkolnikov, G. S. Barron, H. R. Grimsley, N. J. Mayhall, E. Barnes, and S. E. Economou, *PRX Quantum* **2**, 020310 (2021).
- [21] R. Villela, V. S. Prasanna, and B. P. Das, *The European Physical Journal Plus* **137**, 1017 (2022).
- [22] K. Sugisaki, K. Toyota, K. Sato, D. Shiomi, and T. Takui, *The Journal of Physical Chemistry Letters* **12**, 2880 (2021).
- [23] Sumeet, S. Prasanna, V. B. P. Das, and B. K. Sahoo, *Quantum Reports* **4**, 173 (2022).
- [24] K. Bharti *et al.*, *Reviews of Modern Physics* **94**, 015004 (2022).
- [25] M. Motta and J. E. Rice, *Wiley Interdisciplinary Reviews: Computational Molecular Science* **12**, e1580 (2022).
- [26] S. T. Stober, S. M. Harwood, D. Tenev, P. K. Barkoutsos, T. P. Gujarati, and S. Mostame, *Physical Review A* **105**, 012425 (2022).
- [27] R. M. Parrish, E. G. Hohenstein, P. L. McMahan, and T. J. Martínez, *Physical Review Letters* **122**, 230401 (2019).
- [28] V. Zaytsev, M. Groshev, I. Maltsev, A. Durova, and V. Shabaev, *International Journal of Quantum Chemistry* **124**, e27232 (2024).
- [29] L. Veis, J. Višňák, T. Fleig, S. Knecht, T. Saue, L. Visscher, and J. Pittner, *Physical Review A* **85**, 030304 (2012).
- [30] T. F. Stetina, A. Ciavarella, X. Li, and N. Wiebe, *Quantum* **6**, 622 (2022).
- [31] K. Sugisaki, V. Prasanna, S. Ohshima, T. Katagiri, Y. Mochizuki, B. Sahoo, and B. Das, *Electronic Structure* **5**, 035006 (2023).
- [32] V. Kumar, N. Baskaran, V. S. Prasanna, K. Sugisaki, D. Mukherjee, K. G. Dyllal, and B. P. Das, *Physical Review A* **109**, 042808 (2024).
- [33] P. Pyykkö and J. P. Desclaux, *Accounts of Chemical Research* **12**, 276 (1979).
- [34] R. Ahuja, A. Blomqvist, P. Larsson, P. Pyykkö, and P. Zaleski-Ejgierd, *Physical Review Letters* **106**, 018301 (2011).
- [35] T. Chupp, P. Fierlinger, M. Ramsey-Musolf, and J. Singh, *Reviews of Modern Physics* **91**, 015001 (2019).
- [36] N. Yamanaka, B. Sahoo, N. Yoshinaga, T. Sato, K. Asahi, and B. Das, *The European Physical Journal A* **53**, 1 (2017).
- [37] B. Ohayon, R. G. Ruiz, Z. Sun, G. Hagen, T. Papenbrock, and B. K. Sahoo, *Physical Review C* **105**, L031305 (2022).
- [38] B. Ohayon, J. Padilla-Castillo, S. Wright, G. Meijer, and B. Sahoo, *arXiv preprint arXiv:2402.07618* (2024).
- [39] B. Sahoo, B. Das, and H. Spiesberger, *Physical Review D* **103**, L111303 (2021).
- [40] Z.-M. Tang, Y.-m. Yu, B. Sahoo, C.-Z. Dong, Y. Yang, and Y. Zou, *Physical Review A* **107**, 053111 (2023).
- [41] M. Safronova, D. Budker, D. DeMille, D. F. J. Kimball, A. Derevianko, and C. W. Clark, *Reviews of Modern Physics* **90**, 025008 (2018).
- [42] V. Prasanna, A. Vutha, M. Abe, and B. Das, *Physical Review Letters* **114**, 183001 (2015).
- [43] A. Sunaga, V. Prasanna, M. Abe, M. Hada, and B. Das, *Physical Review A* **99**, 040501 (2019).
- [44] L. F. Pašteka, E. Eliav, A. Borschevsky, U. Kaldor, and P. Schwerdtfeger, *Physical review letters* **118**, 023002 (2017).
- [45] A. A. Borschevsky, M. Iliáš, V. A. Dzuba, V. V. Flambaum, and P. Schwerdtfeger, *Physical Review A—Atomic,*

- Molecular, and Optical Physics **88**, 022125 (2013).
- [46] P. A. B. Haase, E. Eliav, M. Ilias, and A. Borschevsky, *The Journal of Physical Chemistry A* **124**, 3157 (2020).
- [47] T. Mishra, R. V. Pai, S. Ramanan, M. S. Luthra, and B. P. Das, *Physical Review A* **80**, 043614 (2009).
- [48] E. B. Norrgard, D. J. McCarron, M. H. Steinecker, M. R. Tarbutt, and D. DeMille, *Physical Review Letters* **116**, 063004 (2016).
- [49] A. C. Vutha *et al.*, *Journal of Physics B: Atomic, Molecular and Optical Physics* **43**, 074007 (2010).
- [50] Y. Gao and T. Gao, *Physical Review A* **90**, 052506 (2014).
- [51] R. Pang *et al.*, *ACS Omega* **8**, 19391 (2023).
- [52] R. L. McNally, I. Kozyryev, S. Vazquez-Carson, K. Wenz, T. Wang, and T. Zelevinsky, *New Journal of Physics* **22**, 083047 (2020).
- [53] S. Vázquez-Carson, Q. Sun, J. Dai, D. Mitra, and T. Zelevinsky, *New Journal of Physics* **24**, 083006 (2022).
- [54] H. Shang, X. Zeng, M. Gong, Y. Wu, S. Guo, H. Qian, C. Zha, Z. Fan, K. Yan, X. Zhu, *et al.*, arXiv preprint arXiv:2405.09164 (2024).
- [55] S. Sun, C. Kumar, K. Shen, E. Shishenina, and C. B. Mendl, Evaluating ground state energies of chemical systems with low-depth quantum circuits and high accuracy (2024), arXiv:2402.13960 [quant-ph].
- [56] G. R. Dahale, in *2023 IEEE International Conference on Quantum Computing and Engineering (QCE)*, Vol. 2 (IEEE, 2023) pp. 89–93.
- [57] L. Zhao, J. J. Goings, K. Shin, W. Kyoung, J. I. Fuks, J.-K. K. Rhee, Y. M. Rhee, K. Wright, J. H. V. Nguyen, J. Kim, and S. Johri, *npj Quantum Information* **9**, 1 (2022).
- [58] C. Sarma, O. Di Matteo, A. Abhishek, and P. C. Srivastava, *Physical Review C* **108**, 064305 (2023).
- [59] L. Zhao, Q. Wang, J. J. Goings, K. Shin, W. Kyoung, S. Noh, Y. M. Rhee, and K. Kim, *npj Quantum Information* **10**, 76 (2024).
- [60] P. J. Ollitrault *et al.*, *Physical Review Research* **2**, 043140 (2020).
- [61] M. Abe, G. Gopakumar, M. Hada, B. P. Das, H. Tatewaki, and D. Mukherjee, *Physical Review A* **90**, 022501 (2014).
- [62] J. T. Seeley, M. J. Richard, and P. J. Love, *The Journal of Chemical Physics* **137**, 224109 (2012).
- [63] N. M. Fazil, V. S. Prasanna, K. V. P. Latha, M. Abe, and B. P. Das, *Physical Review A* **98**, 032511 (2018).
- [64] N. M. Fazil, V. S. Prasanna, K. V. P. Latha, M. Abe, and B. P. Das, *Physical Review A* **99**, 052502 (2019).
- [65] DIRAC, a relativistic ab initio electronic structure program, Release DIRAC22 (2022), written by H. J. Aa. Jensen *et al.* (available at <http://dx.doi.org/10.5281/zenodo.6010450>, see also <http://www.diracprogram.org>).
- [66] M. Treinish *et al.*, Qiskit: An open-source framework for quantum computing (2022).
- [67] K. G. Dyall, *The Journal of Physical Chemistry A* **113**, 12638 (2009).
- [68] D. Kraft, *A Software Package for Sequential Quadratic Programming* (Wiss. Berichtswesen d. DFVLR, 1988).
- [69] J. R. McClean *et al.*, *Quantum Science and Technology* **5**, 034014 (2020).
- [70] C. Cao *et al.*, *Physical Review A* **105**, 062452 (2022).
- [71] Y. Fan, C. Cao, X. Xu, Z. Li, D. Lv, and M.-H. Yung, *The Journal of Physical Chemistry Letters* **14**, 9596 (2023).
- [72] S. Sivarajah, S. Dilkes, A. Cowtan, W. Simmons, A. Edgington, and R. Duncan, *Quantum Science and Technology* **6**, 014003 (2020).
- [73] A. Kissinger and J. van de Wetering, in *Proceedings 16th International Conference on Quantum Physics and Logic*, Chapman University, Orange, CA, USA., 10-14 June 2019, *Electronic Proceedings in Theoretical Computer Science*, Vol. 318, edited by B. Coecke and M. Leifer (Open Publishing Association, 2020) pp. 229–241.
- [74] J. Riu, J. Nogué, G. Vilaplana, A. Garcia-Saez, and M. P. Estarellas, Reinforcement learning based quantum circuit optimization via ZX-calculus (2024), arXiv:2312.11597 [quant-ph].
- [75] C. Holker, Causal flow preserving optimisation of quantum circuits in the zx-calculus (2024), arXiv:2312.02793 [quant-ph].
- [76] A. Maksymov, J. Nguyen, Y. Nam, and I. Markov, Enhancing quantum computer performance via symmetrization (2023), arXiv:2301.07233 [quant-ph].
- [77] X. Bonet-Monroig, R. Sagastizabal, M. Singh, and T. E. O’Brien, *Physical Review A* **98**, 062339 (2018).
- [78] J. Goings, L. Zhao, J. Jakowski, T. Morris, and R. Pooser, in *2023 IEEE International Conference on Quantum Computing and Engineering (QCE)* (IEEE Computer Society, Los Alamitos, CA, USA, 2023) pp. 76–82.

Table S1. Table presenting the ground state energies and PDMs (includes frozen core and nuclear contributions along with the active space contribution) of the considered molecules from different methods. The list of abbreviations used are HF: Hartree–Fock, DHF: Dirac–Hartree-Fock, VQE: VQE with UCCSD ansatz, NR: non-relativistic, Rel: relativistic, CASCI: Complete Active Space Configuration Interaction. Our main results for this work are marked in bold font. The energy is in units of Hartree, whereas the PDM is given in atomic units.

Molecule	Method	Energy	PDM
BeH	HF	-15.153224	0.1137
	DF	-15.156052	0.1137
	VQE (NR)	-15.155941	0.0936
	VQE (Rel)	-15.158768	0.0937
	CASCI (NR)	-15.155949	0.0933
	CASCI (Rel)	-15.158776	0.0933
MgH	HF	-200.157231	0.5850
	DF	-200.477277	0.5861
	VQE (NR)	-200.159639	0.5288
	VQE (Rel)	-200.479695	0.5295
	CASCI (NR)	-200.159665	0.5287
	CASCI (Rel)	-200.479722	0.5294
CaH	HF	-677.314268	0.8269
	DF	-680.265163	0.8374
	VQE (NR)	-677.315076	0.8020
	VQE (Rel)	-680.265994	0.8111
	CASCI (NR)	-677.315085	0.8061
	CASCI (Rel)	-680.266003	0.8150
SrH	HF	-3132.103015	0.9829
	DF	-3178.633202	1.0331
	VQE (NR)	-3132.103414	0.9650
	VQE (Rel)	-3178.633645	1.0119
	CASCI (NR)	-3132.103417	0.9701
	CASCI (Rel)	-3178.633649	1.0165
BaH	HF	-7884.116035	0.9510
	DF	-8136.206375	1.0843
	VQE (NR)	-7884.116240	0.9400
	VQE (Rel)	-8136.206603	1.0715
	CASCI (NR)	-7884.116240	0.9446
	CASCI (Rel)	-8136.206609	1.0755
RaH	HF	-23094.880586	1.1306
	DF	-25028.736164	1.5383
	VQE (NR)	-23094.880796	1.1159
	VQE (Rel)	-25028.736452	1.5177
	CASCI (NR)	-23094.880796	1.1203
	CASCI (Rel)	-25028.736502	1.5180

Table S2. Table presenting the PDMs (includes frozen core and nuclear contributions along with the active space contribution) in the relativistic regime of the molecules considered for Hardware execution. The PDM is given in atomic units.

Molecule	Method	PDM
SrH (12 <i>q</i>)	DF	1.3695
	UCCSD	0.9828
	CASCI	0.9729
	UCCSD(1<i>θ</i>*)	1.3402
	Hardware	1.1655
SrH (6 <i>q</i>)	DF	1.3695
	UCCSD	1.3410
	CASCI	1.3247
	UCCSD(1<i>θ</i>*)	1.3636
	Hardware	1.0293
SrF (6 <i>q</i>)	DF	1.6145
	UCCSD	1.5910
	CASCI	1.5755
	UCCSD(1<i>θ</i>*)	1.6099
	Hardware	1.1978

Table S3. Table presenting the clique-wise contribution to PDM at HF and correlated levels for SrH (6- and 12-spinorbital active space denoted as ‘6q’ and ‘12q’ respectively) and SrF (6-spinorbital space) with 1-parameter VQE statevector calculation. For this case, the entire contribution to the PDM, both at mean field level and correlated level, comes from Pauli strings containing only I and Z . For a given molecule, each row is a clique (qubit-wise commuting), and lists the number of Pauli words in each clique.

Molecule	Terms	$\langle \Phi_0 \hat{D} \Phi_0 \rangle$	$\langle \Psi _r \hat{D} \Psi \rangle_r$	Correlation in PDM (a.u.)
SrH (6q)	IIIII , IIIIZ, IIIZI, IIZII, IIZII, IZIII, ZIIII	6.75406	6.75997	0.00591
	IIIIY, IIIYI, IYIII, YIIII	0	0	0
	IIIXX, IIXXI, IXXII, XXIII	0	0	0
	IIYZY, YZYII	0	0	0
	IIXZX, XZXII	0	0	0
SrF (6q)	IIIII , IIIIZ, IIIZI, IIZII, IIZII, IZIII, ZIIII	5.96841	5.97296	0.00455
	IIIIY, IIIYI, IYIII, YIIII	0	0	0
	IIIXX, IIXXI, IXXII, XXIII	0	0	0
	IIYZY, YZYII	0	0	0
	IIXZX, XZXII	0	0	0
SrH (12q)	IIIIIIIIII , IIIIIIIIZ, IIIIIIIIZI IIIIIIIZII, IIIIIIIIZII, IIIIIIIIZII IIIIIIIZIII, IIIIIIIIZIII, IIIIIIIIZIII IIIIIIIZIIII, IIIIIIIIZIIII, IIIIIIIIZIIII ZIIIIIIIIII	14.81738	14.84663	0.0292
	IIIIIIIIYY, IIIIIIIYYI, IIIIIIIYYII IIIIIIYZYII, IIIIIIIYZYII, IIIIIIIYZYII IIIIIIYZYII, YZYIIIIII	0	0	0
	IIIIIIIXX, IIIIIIIIXXI, IIIIIIIIXXII IIIIIIIXXIII, IIIIIIIIXXIII, IIIIIIIIXXIII IIIIIIIXXIII, XZXIIIIII	0	0	0
	IIIIIIYZY, IIIIIIIYZYII, IIIIIIIYZYIII, YZZYIIIIII	0	0	0
	IIIIIIIXZX, IIIIIIIIXZXII, IIIIIIIIXZXIII, XZZXIIIIII	0	0	0
	IIIIIIYZZY, IYZZYIIIIII	0	0	0
	IIIIIIIXZX, IIXZXIIIIII	0	0	0
	IIIIIIYZZZY, YZZZYIIIIII	0	0	0
	IIIIIIIXZZX, XZZZXIIIIII	0	0	0
	IIIIIIYZYI, IYZYIIIIII	0	0	0
	IIIIIIIXZXI, IIXZXIIIIII	0	0	0
	IIIIIIYZZYI, YZZZYIIIIII	0	0	0
	IIIIIIIXZZXI, XZZZXIIIIII	0	0	0